ARTICLE INFO
Article ID: 03-12-02-0015

doi:10.4271/03-12-02-0015

A Comparison of EGR Correction Factor Models Based on SI Engine Data

Jamie Karl Smith and Daniel Ruprecht, *University of Leeds, UK*
Philip John Roberts, *Horiba MIRA, UK*
Alexandros Kountouriotis and Pavlos Aleiferis, *Imperial College London, UK*
David Richardson, *Jaguar Land Rover, UK*

Abstract

The article compares the accuracy of different exhaust gas recirculation (EGR) correction factor models under engine conditions. The effect of EGR on the laminar burning velocity of a EURO VI E10 specification gasoline (10% Ethanol content by volume) has been back calculated from engine pressure trace data, using the Leeds University Spark Ignition Engine Data Analysis (LUSIEDA) reverse thermodynamic code. The engine pressure data ranges from 5% to 25% EGR (by mass) with the running conditions, such as spark advance and pressure at intake valve closure, changed to maintain a constant engine load of 0.79 MPa gross mean effective pressure (GMEP). Based on the experimental data, a correlation is suggested on how the laminar burning velocity reduces with increasing EGR mass fraction. This correlation, together with existing models, was then implemented into the quasi-dimensional Leeds University Spark Ignition Engine (LUSIE) predictive engine code and resulting predictions are compared against measurements. It was found that the new correlation is in good agreement with experimental data for a diluent range of 5%-25%, providing the best fit for both engine loads investigated, whereas existing models tend to overpredict the reduction of burning velocity due to EGR.

History

Received: 06 Aug 2018
Revised: 07 Nov 2018
Accepted: 06 Feb 2019
e-Available: 27 Mar 2019

Keywords

EGR, SI Engine, Thermodynamic modelling, Laminar burning velocity,

Citation

Smith, J., Roberts, P., Kountouriotis, A., Richardson, D. et al., "A Comparison of EGR Correction Factor Models Based on SI Engine Data," *SAE Int. J. Engines* 12(2):203–217, 2019, doi:10.4271/03-12-02-0015.

ISSN: 1946-3936
e-ISSN: 1946-3944

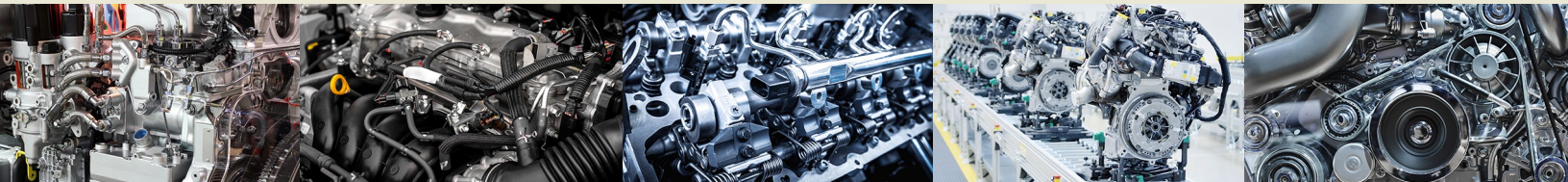

Introduction

Government legislation on controlling emissions from combustion engine powered vehicles is becoming ever more stringent. Therefore, car manufacturers have to keep improving their engines to minimise fuel consumption and emissions. The latest European regulations (EURO VI) came into effect in 2014 and focus primarily on reducing nitrogen oxide (NO_x). An effective strategy to reduce NO_x emissions is to use Exhaust Gas Recirculation (EGR), that is, to recirculate cooled exhaust gas into the cylinder. High levels of EGR have been found to reduce not only NO_x emissions but carbon monoxide (CO), particulate mass (PM) and particulate number (PN) [1, 2, 3]. EGR has also been found to reduce the chances of auto-ignition due to lower end gas temperatures [4, 5, 6, 7, 8]. The reduction in end gas temperature also allows the compression ratio to be increased, leading to improved engine efficiency [9].

The fact that cooled EGR leads to a decrease in laminar burning velocity is well known. Therefore, in computer simulations of combustion engines, the effect of EGR is typically modelled through a correction factor that reduces laminar burning velocity depending on the applied level of EGR. A variety of different models have been suggested, but none of them are based on engine-like conditions. A summary of the conditions at which published correlation were determined is presented in Table 1.

The correction factor proposed by Metghalchi and Keck [10] was found experimentally, using a constant volume combustion chamber at an initial pressure of 0.1 MPa, for a stoichiometric mixture of isooctane and air for an unburned gas temperature range of 340-440K. The composition of diluent to simulate combustion products was 15% carbon dioxide and 85% nitrogen by volume.

Their model was later modified by Rhodes and Keck [11] for a blended fuel similar to gasoline, known as indolene. Because of the change in mixture, the composition of the diluent was altered to simulate combustion products, with the diluent now containing 20% carbon dioxide and 80% nitrogen by volume. The correction factor was determined for an equivalence ratio of 0.7-1.2 and for initial pressures of 0.1 and 0.2 MPa.

A correlation purely based on simulations was determined by Fu et al. [12] using the CHEMKIN-PRO software and the Frassoldati et al. model [13], which contains 249 species and 7966 reactions. The laminar burning velocity simulations were carried out at pressures and temperatures of up to 0.5 MPa and 500 K, respectively, for a stoichiometric mixture. However, the running conditions at which the EGR correction factor was determined are unclear. The diluent composition is user defined and includes carbon dioxide, nitrogen and water.

The most recently suggested correction factor is based on a combination of simulations and experiments. Bhattacharya et al. [14] used a commercial gasoline (Shell V-Power as available in Germany) that, given the publication date of the paper, should be compliant with EURO VI regulations. For the experimental data, Bhattacharya et al. used a heat flux burner to determine the stretch free laminar burning velocities with the diluent comprising of carbon dioxide and nitrogen. Simulations were performed using the CHEMKIN-PRO package and a chemical mechanism constituting 877 reactions and 171 species [15]. This mechanism has been derived from a more complex mechanism containing 3796 reactions and 874 species [16, 17]. The chemical model was validated against the burner experimental data, and a correlation for the EGR correction factor was proposed. Both experimental and numerical data was taken at a pressure of 0.1 MPa and unburned gas temperature of 432 K.

Another recent study on the effects of exhaust gas recirculation of a fuel for a advanced combustion engine (FACE-C) has found that the laminar burning velocity decreases quasi-linearly as the levels of EGR increases [18] but does not specify a correction factor.

Currently, to the best of the authors' knowledge, no work exists that compares these models in terms of their accuracy under engine conditions. Middleton et al. [19] simulated the effect of EGR on the laminar burning velocity of isooctane air mixtures at high pressures (0.1-25 MPa), high temperatures (400-1000 K) and high EGR levels (0%-60% by mass) associated with engine studies. Although operating at engine-like conditions, the study did not directly compare different EGR correction factors.

Therefore, it is not clear which models are useful to simulate the effect of EGR on combustion in SI engines or whether any of them are predictive at all. This is particularly important since recent works [20, 21, 22] have started to look at using very high levels of EGR in combustion engines. To enable robust and reliable computer modelling of the effect of EGR, this article provides a comparison of how well different correction factor models match measurements obtained from an engine.

TABLE 1 Summary of EGR correction factor correlations.

Model	Method	Pressure (MPa)	Temperature (K)	ϕ
Metghalchi and Keck	Combustion bomb	0.1	320-440	1.0
Rhodes and Keck	Combustion bomb	0.1-0.2	350-550	0.7-1.2
J. Fu et al. (isooctane)	Numerical simulation	0.5	500	1.0
Bhattacharya et al.	Burner and Numerical simulation	0.1	423	0.7-1.3
Present study	Engine data	3.0	768	1.0

It also provides the first derivation of a correction factor directly from engine data. Using the Leeds University Spark Ignition Engine Data Analysis (LUSIEDA) software, we back calculate a correction factor for EGR levels of up to 25%. While this back-calculating approach comes with challenges regarding the proper choice of model parameters, by relying on engine data it captures the effects of the full composition of exhaust gas. The obtained correlation is then implemented into a quasi-dimensional predictive model and compared to the models mentioned above to see which one results in the best fit to the measured pressure trace. We show that while all models provide reasonably good agreement with experimental data at low levels of EGR (5%-10%), only the new found correction factor can match the measured pressure traces and mass fraction burned at higher levels of EGR (20%-25%) as existing models overestimate the reduction in laminar burning velocity due to the effects of EGR to varying degree.

Methodology

Both the forward model LUSIE (Leeds University Spark Ignition Engine) and the backward model LUSIEDA (Leeds University Spark Ignition Engine Data Analysis) are quasi-dimensional thermodynamic codes separating the combustion chamber into at least two zones. LUSIE is predictive, modelling pressure traces for specific engine conditions. In contrast, LUSIEDA is a reverse thermodynamic code that back calculates combustion parameters, such as the mass fraction burned, turbulent mass burning velocity and burned gas radius, from experimentally obtained in-cylinder engine pressure data.

In the first part of the article, we used LUSIEDA to back calculate burning velocities from pressure data to find the EGR correction factor correlation from experimental pressure traces in the engine for varying levels of EGR (see Experimental set-up section). Then, the new-found correlation as well as the four existing correction factor models in Table 1 were implemented into the predictive combustion code LUSIE to compute predicted pressure traces. Those were then compared against the original pressure data as well as a second set of data obtained under different running conditions to assess their suitability as a predictive model under engine conditions.

Experimental Set-Up

The engine from which experimental data was taken was a Single Cylinder Research Engine (SCRE) version of the latest Jaguar Land Rover gasoline Ingenium engine, housed at Imperial College London. A geometrical specification of the SCRE is shown in Table 2.

A full description of the engine, ancillaries, sub-systems and experimental methodology is available in the published literature [23, 24].

TABLE 2 Jaguar Land Rover SCRE specification.

Parameter	Value
Displaced volume [cc]	499.02
Compression ratio	10.86
Number of cylinders	1
Number of valves	4
Fuel injection	Central DI
Intake maximum opening point [°CA aTDCgx]	161
Exhaust maximum opening point [°CA bTDCgx]	121
Intake phaser range [°CA]	50
Exhaust phaser range [°CA]	50

As engine pressure trace data is used to derive the EGR correction factor correlation, the accuracy of the pressure data is important. A description of the pressure acquisition and associated errors is given by Smith et al. [23], stating that "High speed, crank angle resolved data was recorded using AVL Indicom v2.6 as part of an AVL Indiset Advanced Gigabit unit utilising a 14-bit analogue to digital convertor (maximum error of ±0.95 kPa, ±0.061 kPa and ±0.122 kPa for the in-cylinder, intake and exhaust pressure channels). A water-cooled Kistler 6041B piezo-electric sensor (accurate to <1% of full scale), mounted flush with the combustion chamber surface, in combination with a Kistler 5064 charge amplifier were used to measure in-cylinder pressure. This 'dynamic' pressure was referenced to the intake manifold pressure (measured using a Kistler 4007 type sensor in conjunction with a Kistler 4665 signal conditioner) measured at the crank angle equidistant between the crank angles of maximum valve lift and intake valve closure."

EGR was used throughout the duration of the currently reported study. By definition, the EGR rate was calculated as the ratio of the carbon dioxide measured within the intake manifold to the carbon dioxide content measured in the exhaust stream; both intake and exhaust CO_2 was measured using a Horiba MEXA One emissions analyser. EGR rate was calculated by the MEXA with the result being output to the data acquisition system.

When required, EGR was sampled via a low-pressure loop system which resulted in EGR being introduced downstream of the intake air filter but upstream of a split in the intake system that was required to "switch" the single cylinder engine from running under naturally aspirated or boosted conditions. The hot EGR was cooled using a Ford DW12 water-cooled EGR cooler with the rate being controlled via a Ford DW12 EGR valve.

Under naturally aspirated conditions, EGR was combined with the intake air before passing through a heat exchanger where the intake charge (air and EGR) temperature was controlled to 45°C, accurate to ±1°C, measured at the intake plenum. Under boosted conditions, intake air and EGR were combined at the same point in the intake system before they were passed through an Eaton V240 supercharger. The same heat exchanger described above was then used to "cool" the intake charge mixture to 45°C ± 1°C, measured at the intake plenum.

To control the desired EGR rate, a closed-loop EGR rate control system was developed which allowed the user to define an EGR rate input, with the output defined as the measured EGR rate with the control functionality applied to the EGR valve.

Whilst the level of EGR introduced to the engine is typically very easy to quantify (using the methodology described previously), it is more difficult but not impossible to measure the quantity of residual gas left over in the chamber after combustion. In a paper by Peckham et al. [25], in-cylinder residual concentration was measured using in-cylinder Non-Dispersive Infra Red (NDIR) analysers that allowed crank-resolved measurements of CO and CO_2 and thus the calculation of the in-cylinder residual content. However, without this type of specialized equipment, in-cylinder residual concentration is typically quantified using 1D or CFD simulations.

Residual values typically vary from 5% to 15% with the residual concentration being influenced by valve overlap. Advantages of trapped residuals include a decrease in the generation of in-cylinder NO_x emissions and a reduction in pumping losses, whereas disadvantages include an increase in the production of particulate matter and increased cycle-to-cycle variation. Throughout the duration of the currently reported study, the crank angles of maximum opening for both intake and exhaust valves remained constant ensuring valve overlap and thus the level of trapped in-cylinder residuals remained broadly constant.

The effect of residuals in the forward model is accounted for by the model parameters for the 0% EGR case in the predictive engine simulations.

Backward Model

The EGR correction factor is defined as

$$\text{EGR correction factor} = \frac{u_l(f)}{u_l(f=0)} \qquad \text{Eq. (1)}$$

where f is the mass fraction of EGR, $u_l(f)$ the laminar burning velocity with EGR and $u_l(f=0)$ the laminar burning velocity without EGR. Therefore, to determine the correction factor from data, we need to determine u_l for different levels of EGR and the no-EGR baseline. The in-cylinder residuals were calculated using the model suggested by Cho et al. [26] and included the back calculation to ensure that the unburned gas density was accurate. The hot residuals also effect the in-cylinder temperature at IVC for both the backwards and predictive model.

Several models exist in the literature that link the laminar burning velocity with the turbulent burning velocity using a correlation

$$u_t \propto u_l^x \qquad \text{Eq. (2)}$$

with x being a model-dependent constant. In predictive simulations u_t is computed from u_l. For back-calculation, in contrast, we rearrange the model to find the laminar burning velocity from the turbulent burning velocity determined from pressure data. The full process is shown as a flowchart in Figure 1.

FIGURE 1 Flowchart describing process of obtaining EGR correction factor from engine pressure trace data.

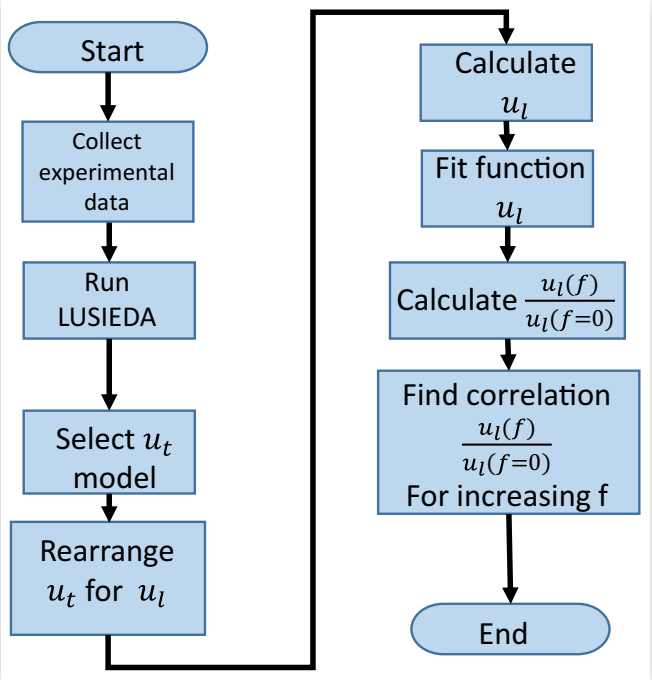

LUSIEDA calculates the pressure rise inside the combustion chamber incrementally during combustion:

$$P_{i+1} = P_i + \Delta P_m + \Delta P_{ht} + \Delta P_{bb} + \Delta P_{comb} \qquad \text{Eq. (3)}$$

where P_i and P_{i+1} are experimental pressure data at two consecutive crank angles, ΔP_m is the change in pressure due to isentropic compression/expansion, ΔP_{ht} is the change in pressure due to heat transfer, ΔP_{bb} is the change in pressure due to blow-by and ΔP_{comb} is the change in pressure due to combustion. The heat transfer and blow-by in this study (reverse and forward modelling) is calculated using the Woschni [27] and a "flow through orifice" model [28], respectively. An iterative method is used to determine the change in mass burned, Δm_b, required for ΔP_{comb} to equal the measured value found from Equation 3. The change in mass burned can then be used to calculate the turbulent mass burning velocity, u_{tr}, from

$$\frac{\Delta m_b}{\Delta t} = \rho_u A_f u_{tr} \qquad \text{Eq. (4)}$$

where ρ_u is the unburned gas density and A_f is the burned gas area. The burned gas area is calculated by assuming a spherically propagating flame that is truncated by the cylinder. Currently, the backwards model assumes idealised pent chamber geometry, while the predictive model has been

developed to accommodate for real engine geometry. LUSIEDA iterates to find a burned gas radius and uses this information to determine the area of the burned gas. Note that LUSIEDA uses a two-zone model approach which assumes that entrained fuel is burned instantaneously. This is because experimental pressure trace data does not allow flame front information to be computed, instead requiring additional optical data which is not readily available in an engine. The reverse analysis approach adopted here has been widely used in engine modelling [29, 30, 31, 32].

Turbulent Burning Velocity Model

The original Zimont model describes a flame which transitions from a laminar flame to the thin reaction zone and wrinkled flame of the flamelet region and eventually to a region where the flame brush thickens [33]. The Zimont model reads:

$$u_{t0} = Au'\mathrm{Da}^{1/4} \qquad \text{Eq. (5)}$$

where u_{t0} is the fully developed turbulent burning velocity, A is a user defined constant, u' is the turbulent RMS velocity and Da is the Damköhler number. The Zimont model was updated to the Zimont-Lipatnikov model through the inclusion of a flame development factor and an extra laminar burning velocity term, u_l, to correct for when the turbulence approached zero [34]. The Zimont-Lipatnikov model reads:

$$u_{tr} = u_l + Au_k'\mathrm{Da}^{1/4} \qquad \text{Eq. (6)}$$

where u_k' is the flame development factor multiplied by the turbulent RMS velocity, also known as the effective turbulent RMS velocity. In the back calculation of the correction factor, for the sake of simplicity, we use the mean u_{tr} value over all experimental pressure traces instead of running 300 instances of the backward model and averaging those. The Damköhler number, Da, depends on the laminar burning velocity:

$$\mathrm{Da} = \frac{\tau_t}{\tau_c} = \frac{Lu_l^2}{u'\kappa} \qquad \text{Eq. (7)}$$

where τ_t is the turbulence time scale, τ_c is the chemical time scale, L is the integral length scale of turbulence and κ is the thermal diffusivity. The parameters L and u' for the studied engine were determined using CFD simulations [23] and were parsed into the code from an ASCII file. The turbulence parameters are crank resolved and the corresponding values are called at each time step. The turbulence parameters are used in calculating the turbulent burning velocity and to determine the rate of mass burned in the three zone model. Substituting Equation 7 into Equation 6 and rearranging for u_l gives:

$$u_l = 0.5 \cdot \left(Z^2 - \left(Z^4 + 4Z^2 \cdot u_{tr} \right)^{0.5} + 2u_{tr} \right) \qquad \text{Eq. (8)}$$

where Z is:

$$Z = Au_k' \left(\frac{L}{u'\kappa} \right)^{0.25} \qquad \text{Eq. (9)}$$

In predictive simulations using the forward model, the constant A is fixed by tuning the model to measurements. This is not possible for the backward model but we can fix A to match more recently published models for the turbulent burning velocity. Recent research showed that the turbulent burning velocity depends on the stretch rate Markstein number, Ma_{sr}, and the Karlovitz stretch factor [35, 36]. Their model, which we refer to as the U/K correlation, reads

$$\frac{u_t}{u_k'} = U = \alpha \cdot K^{\beta} \qquad \text{Eq. (10)}$$

and is derived experimentally for a number of different fuels, over a range of pressures and temperatures. For positive Markstein numbers, we have

$$\alpha = 0.023\left(30 - \mathrm{Ma}_{sr}\right) \qquad \text{Eq. (11a)}$$

$$\beta = 0.0103\left(\mathrm{Ma}_{sr} - 30\right) \qquad \text{Eq. (11b)}$$

whereas for negative Markstein numbers

$$\alpha = 0.085\left(7 - \mathrm{Ma}_{sr}\right) \qquad \text{Eq. (12a)}$$

$$\beta = -0.0075\left(\mathrm{Ma}_{sr} + 30\right). \qquad \text{Eq. (12b)}$$

Since the Markstein number is dependent upon the mixture composition, temperature and pressure, making direct use of their correlation in the backward model is challenging. No data exists in the literature about this dependence at the temperatures and pressures experienced in an Internal Combustion Engine (ICE). Furthermore, there is also no data regarding a similar fuel to that used in the present study or the effect that increasing levels of EGR diluent has on Ma_{sr}.

However, we can fix the constant A in the Zimont-Lipatnikov model so that it closely aligns with the U/K correlation for a given Markstein number. The Damköhler number is inversely proportional to the Karlovitz stretch factor, with an extra factor to account for the difference in turbulence length scales used:

$$\mathrm{Da} = K^{-1} \cdot \frac{L}{\lambda} \qquad \text{Eq. (13)}$$

where λ is the Taylor microscale. If we ignore the added laminar burning velocity term that accounts for $u' \to 0$, the Zimont-Lipatnikov model becomes:

$$U = A\left(\frac{L}{\lambda}\right)^{1/4} K^{-1/4}. \qquad \text{Eq. (14)}$$

To obtain $\beta = -1/4$ in the U/K correlation (10), we need to set $\mathrm{Ma}_{sr} = 5.73$ in Equation 11b, which in turn means that

FIGURE 2 *U/K* diagram with Zimont-Lipatnikov model plotted.

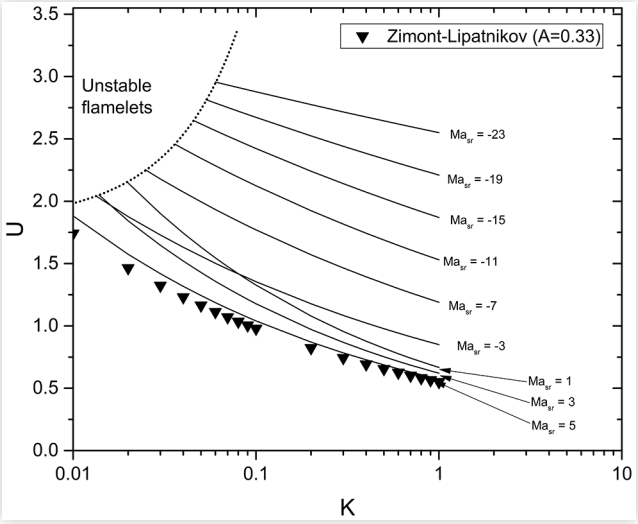

α = 0.558 according to (11a). Note that there is no negative value for Ma_{sr} for which Equation 12b gives $\beta = -1/4$.

The ratio between the integral length scale (obtained from CFD data) and Taylor microscale (computed by the LUSIE model) to the power of –1/4 was calculated for each time step and was found approximately constant with values varying between 0.61 and 0.59. We use the mean value and set

$$\left(\frac{L}{\lambda}\right)^{-1/4} = 0.6. \qquad \text{Eq. (15)}$$

Equating the *U*/K correlation (10) with $\beta = -1/4$ and Equation 14 gives, after cancelling $K^{-1/4}$,

$$\alpha = A\left(\frac{L}{\lambda}\right)^{1/4}. \qquad \text{Eq. (16)}$$

From this, we can now determine a value of *A* that aligns the Zimont-Lipatnikov model with the *U*/*K* correlation:

$$A = \alpha\left(\frac{L}{\lambda}\right)^{-1/4} = 0.558\left(\frac{L}{\lambda}\right)^{-1/4} = 0.33. \qquad \text{Eq. (17)}$$

A plot of the Zimont-Lipatnikov model with $A = 0.33$ is shown in Figure 2. The two models give very similar results and a value of $A = 0.33$ is therefore used for the backward model.

Note that the stretch rate Markstein number for isooctane was found to be around 6 at 0.1 MPa and 358 K [37] with an error of ±1. While our measurements were taken at a higher pressure and higher temperature, it has been shown that increases in pressure will lead to a decrease in Ma_{sr} [37, 38], whereas an increase in temperature leads to an increase in Ma_{sr} [37]. Therefore, the value of $Ma_{sr} = 5.73$ used in this study for gasoline seems reasonable but the lack of data in the literature prevents a more quantitative assessment. Experiments aiming to determine Markstein numbers at high temperatures and pressure would be an important area for future research.

It is worth stressing that the only free parameter in the backwards model is *A* and that the resulting correction factor is not particularly sensitive to it: changing *A* by ±10% was found to have a negligible effect on the back-calculated EGR correction factor, with a maximum change of 1.5% over all EGR values.

Forward Model

The predictive quasi-dimensional model LUSIE splits the combustion chamber into three zones with the extra zone, known as the entrainment zone, based on the work by Blizard and Keck [39]. Fresh gas is entrained into the flame at a rate:

$$\frac{\Delta m_e}{\Delta t} = \rho_u A_{fe} u_{te} \qquad \text{Eq. (18)}$$

where m_e is the mass of gas entrained into the flame brush, A_{fe} is the flame surface area and u_{te} is the turbulent entrainment burning velocity. The rate of mass burned is related to the mass entrained by:

$$\frac{\Delta m_b}{\Delta t} = \frac{m_e - m_b}{\tau_b} \qquad \text{Eq. (19)}$$

where τ_b is the characteristic burn-up time:

$$\tau_b = C_{\tau_b}\frac{\lambda}{u_l} \qquad \text{Eq. (20)}$$

where C_{τ_b} is a constant. LUSIE has been introduced in detail and validated for numerous engines under an array of running conditions in previous publications [23, 30, 40, 41, 42, 43].

The tunable constants within the forward model are the turbulent burning velocity constant, parameter *A* from the Zimont-Lipatnikov model, the characteristic burn-up time constant, C_{τ_b}, and the flame growth time. The turbulent burning velocity constant and characteristic burn-up time constant were tuned for the zero EGR case only.

The flame growth time is tuned to match the 0%-2% mass fraction burned for the simulations. The flame growth time needed to increase (slower early combustion) as the level of EGR increased to avoid the forward model over-predicting the early rate of combustion. For the engine used in the present study, we found that a linear relation between flame growth time and level of EGR worked well. This is analogous to the flame growth multiplier (FGM) factor used in the study by Robertson et al. [44] where it was also found that, as EGR increases, the time taken from 0% to 2% mass fraction burned increased. A more general study of how to model the impact of EGR on kernel delay would be another interesting direction for future research.

Results and Discussion

Laminar burning velocities were calculated using Equation 8 for a range of EGR values from the experimentally derived turbulent burning velocity values. To avoid spark effects and

FIGURE 3 Back-calculated laminar burning velocity plotted against the change in in-cylinder pressure (symbols) and curve fitting of u_l (lines).

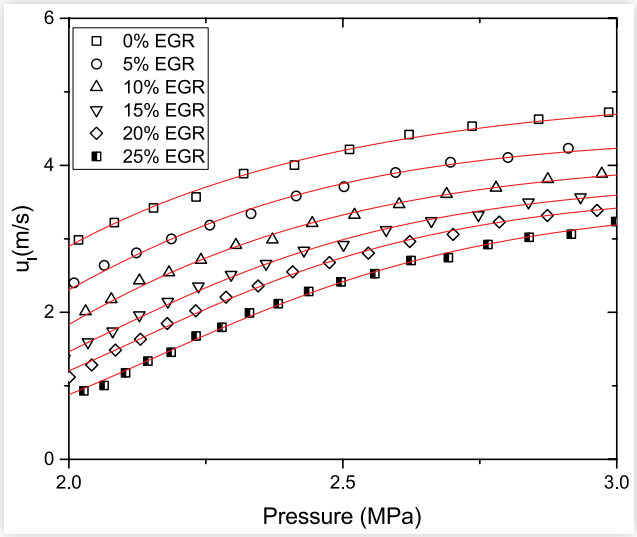

FIGURE 5 Turbulent mass burning velocity plotted against burned gas radius for increasing levels of EGR.

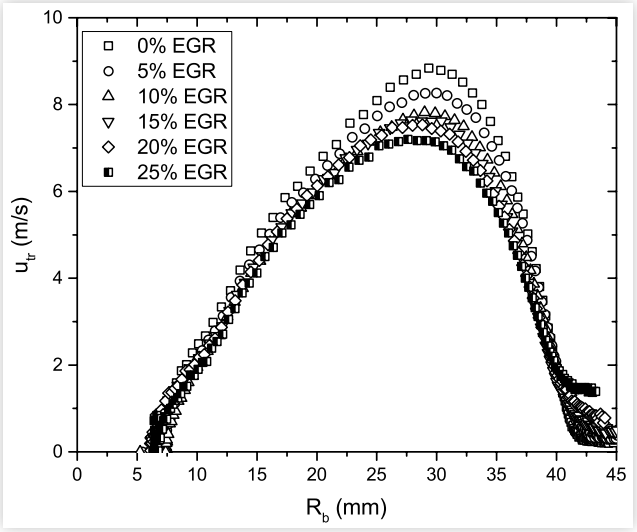

flame deceleration due to interaction with the cylinder walls, the burning velocity measurements were taken when the burned gas radius was 10-30 mm. The back-calculated laminar burning velocity plotted against in-cylinder pressure is shown in Figure 3. A logistic function was used to fit the data points and then to calculate the EGR correction factor for the varying levels of EGR shown in Figure 4.

The calculated EGR correction changes as the flame develops over time and pressure in the cylinder increases. This raises the question at what pressure in Figure 4 the correction factor should properly be chosen. The flame develops in three stages: initial acceleration, then propagation at an approximately constant speed and finally deceleration due to wall effects [29]. The correction factor should account for the impact of EGR on steady-state flame development, whereas the impact on early flame development is modelled by the time taken to form the flame kernel. Figure 5 shows the turbulent mass burning velocity plotted against the burned gas radius. While the steady-state phase with near-constant u_{tr} is not very pronounced in the case studied here, it occurs around the peak of u_{tr} which corresponds to a pressure of 3.0 MPa for the 0% EGR case. Therefore, we determine the proposed correction factor at that pressure value.

FIGURE 4 EGR correction factor plotted against the change in in-cylinder pressure for increasing levels of EGR.

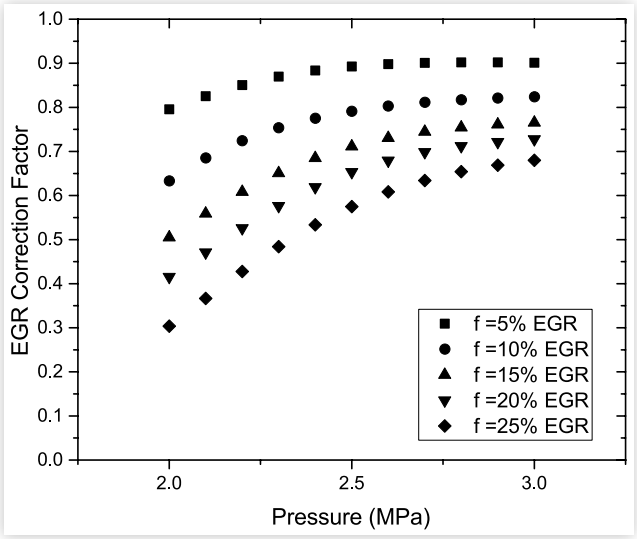

Obtained correction factors are plotted against EGR fraction in Figure 6, together with models from the literature. All models show an approximately linear decrease of the correction factor with EGR. To confirm that the correction factor we derive from data is not sensitive to the number of acquired cycles, we confirmed that when analysing only data from 100 or 200 cycles (in contrast to the full data from 300 cycles used here), the resulting correction factor is very similar to the one shown in Figure 6 (less than 1.5% average difference).

The models by Bhattacharaya et al. and Metghalchi and Keck align very closely. Both the model by Rodes and Keck and by Fu et al. give noticeably smaller correction factors for higher levels of EGR than the first three. The model derived in the present study finds that the EGR correction factor is larger at high levels of EGR compared to the literature. This could be attributed to the composition of the EGR containing species like hydrogen which burn much faster than those included in the simulated EGR within the literature. This is supported by a study by Mannaa et al. [18] who found that synthetic EGR reduced the laminar burning velocity more than real exhaust gas.

FIGURE 6 Correction factor plotted against mass fraction of EGR. The plot compares results from the present study to correction factors found within the literature.

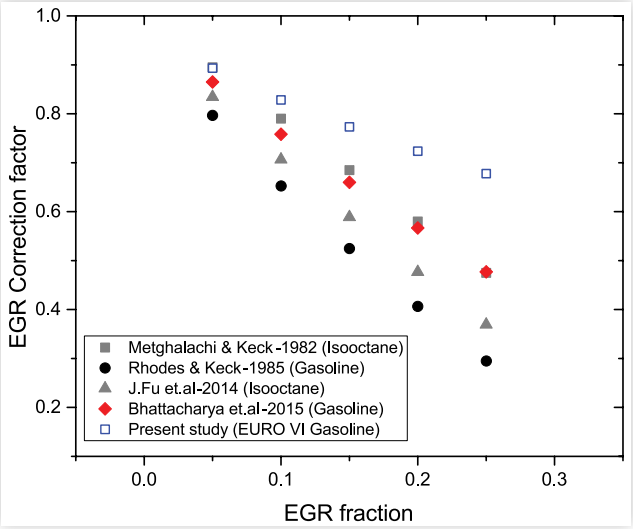

A quasi-linear fit of the data from the present study found that the EGR correction factor changes with the mass fraction of EGR as:

$$\frac{u_l(f)}{u_l(f=0)} = 1 - 0.835\, f^{0.687} \qquad \text{Eq. (21)}$$

where f is the mass fraction of EGR, which was calculated experimentally as the ratio of CO_2 in the intake manifold to the ratio of CO_2 in the exhaust stream. The correlation found in the present study is similar to that suggested by Bhattacharya et al. (for $\phi = 1.0$):

$$\frac{u_l(f)}{u_l(f=0)} = 1 - 1.68\, f^{0.84}. \qquad \text{Eq. (22)}$$

The one by Rhodes and Keck

$$\frac{u_l(f_{mole})}{u_l(f_{mole}=0)} = 1 - 2.06\, f_{mole}^{0.773} \qquad \text{Eq. (23)}$$

where f_{mole} is the mole fraction of EGR has the same functional form but, due to different parameters, leads to significant differences in the obtained correction factors (compare for Figure 6).

The oldest model by Metghalchi and Keck suggests a linear correlation:

$$\frac{u_l(f)}{u_l(f=0)} = 1 - 2.1\, f. \qquad \text{Eq. (24)}$$

We experimented using a linear fit to our data instead of the quasi-linear fit but this led to worse agreement with the measured pressure traces, in particular for low levels of EGR.

The model suggested by Fu et al. is slightly different than the others as it models the components of the diluent individually

$$\frac{u_l(f_{mole})}{u_l(f_{mole}=0)} = 1 - \sum_{i=1}^{n} X_i\, \mu_{1,i}\, f_{mole,i}^{\left(\mu_{2,i}+\mu_{3,i}(\phi-\phi_{m,i})+\mu_{4,i}(\phi-\phi_{m,i})^2\right)} \qquad \text{Eq. (25)}$$

where X_i is the mole fraction of a single component in total diluents, n is the total number of diluents, $\mu_1 - \mu_4$ and ϕ_m are correlation coefficients. For our case ($\phi = 1$), the correlation is given by:

$$\frac{u_l(f_{mole})}{u_l(f_{mole}=0)} = 1 - \left(0.25\, f_{mole}^{0.63} + 0.3\, f_{mole}^{0.8} + 1.5\, f_{mole}^{0.9}\right) \qquad \text{Eq. (26)}$$

where the mole fraction of each diluent was calculated using the isooctane balance equation

$$C_8H_{18} + 12.5(O_2 + 3.76N_2) \rightarrow 8CO_2 + 9H_2O + 47N_2. \qquad \text{Eq. (27)}$$

Forward Modelling

In order to compare how predictive the different correction factor models are, the correlation given by Equation 21 and the models by Metghalchi and Keck, Rhodes and Keck, Fu et al. and Bhattacharya et al. were implemented into the LUSIE forward modelling code. The code was first validated for the case of zero EGR against experimental data consisting of 300 cycles for each running condition.

This data was then divided into fast, middle and slow combustion cycles while removing data in-between these regions. This approach is commonly used when dealing with cyclic variability [40, 42, 45] and allows for a more detailed comparison of the simulated pressure curves. Fast, middle and slow cycle are determined by the peak pressure values, with the fast combustion cycles defined as $P_{max} \geq \bar{P}_{max} + \sigma$, where $\bar{P}_{max}$ is the mean peak pressure value and σ is the standard deviation. The middle cycles are defined as $\bar{P}_{max} - 0.25\sigma \leq P_{max} \leq \bar{P}_{max} + 0.25\sigma$. Finally, slow cycles are defined as $P_{max} \leq \bar{P}_{max} - \sigma$. A validation of the predicted pressure trace for zero EGR against experimental data is shown in Figure 7. The mean experimental pressure trace was calculated by finding the average pressure at each time step (0.1 crank angle degrees) for the 300 cycles. The simulation is in good agreement with experimental data and represents a middle combustion cycle.

The pressure traces and mass fraction burned profiles were then simulated for increasing levels of EGR, ranging from 5% to 25% (by mass) in increments of 5%. For the correlations derived using mole fractions of diluent (Rhodes and Keck and Fu et al.), the mass fraction user input was converted to the mole fraction within the LUSIE code, ensuring the correction factor used the appropriate value of EGR. Figures 8-12 show the simulated pressure traces and mass fraction burned profiles using the different models with

FIGURE 7 Validation of predictive LUSIE for 0% EGR case at engine speed 1500 rpm and engine load of 0.79 MPa GMEP.

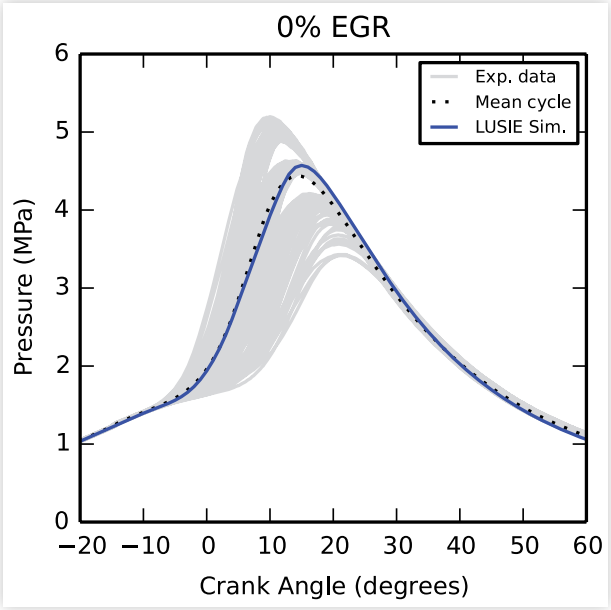

varying levels of diluent. For comparison, the crank-resolved experimental pressure averaged over all 300 cycles is also shown. To avoid clutter, results from the Metghalchi and Keck and Fu et al. model are not shown, but they are relatively close to those from the Bhattacharya et al. and Rhodes and Keck, respectively. Figure 13 shows the root mean square error between simulated and experimental pressure values plotted against level of EGR for all models.

It can be seen that at the lower levels of EGR (5%-10%), all of the correlations provide a reasonable fit to the experimental data although the Rhodes and Keck model predicts a slower combustion cycle. This is somewhat unsurprising as all models give fairly similar correction factor values at 5% EGR as shown in Figure 6.

Substantial differences between models arise as the level of EGR increases to values between 15% and 25%. The very small correction factors in the Rhodes and Keck and Fu et al. models result in an increasingly poor match with experimental data, with errors increasing roughly linearly with EGR level.

The new correlation, the Bhattacharya et al. and Metghalchi and Keck model gives reasonable approximations throughout with similar errors up to around 15% EGR. Bhattacharya et al. and Metghalchi and Keck produce closely aligned pressure traces, tending slightly toward slower cycles for high levels of EGR. The new correlation from the present study improves on these two models for both the 20% and 25% EGR cases predicting pressure trace and mass fraction burned profiles much closer to the mean than any of the models from the literature. The difference at higher levels of EGR is possibly attributed to the diluent composition itself, with the current study recirculating actual exhaust gas as opposed to using a simulated EGR consisting of nitrogen (N_2) for the numerical model and a mixture of nitrogen and carbon dioxide for the heat flux burner and constant volume combustion bomb experiments.

FIGURE 8 Predictive simulations comparing the pressure traces (a) and mass fraction burned (b) at 5% EGR obtained using different EGR correction factor models.

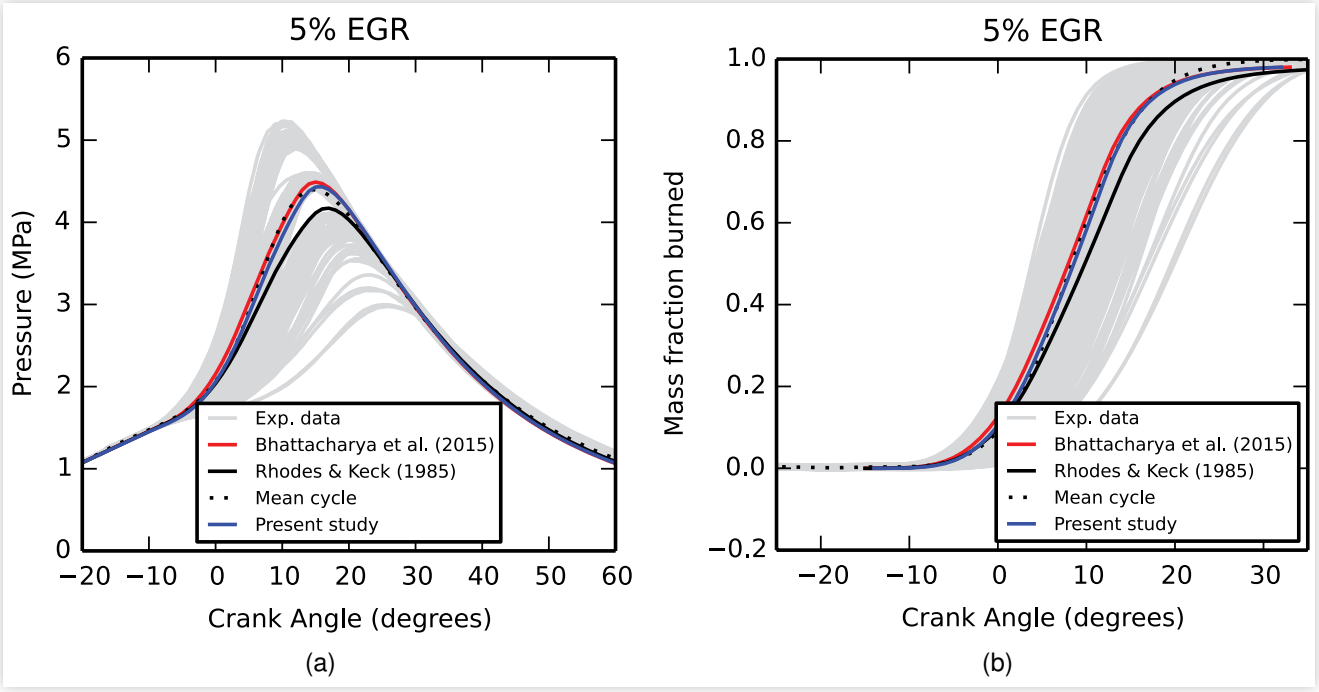

FIGURE 9 Predictive simulations comparing the pressure traces (a) and mass fraction burned (b) at 10% EGR obtained using different EGR correction factor models.

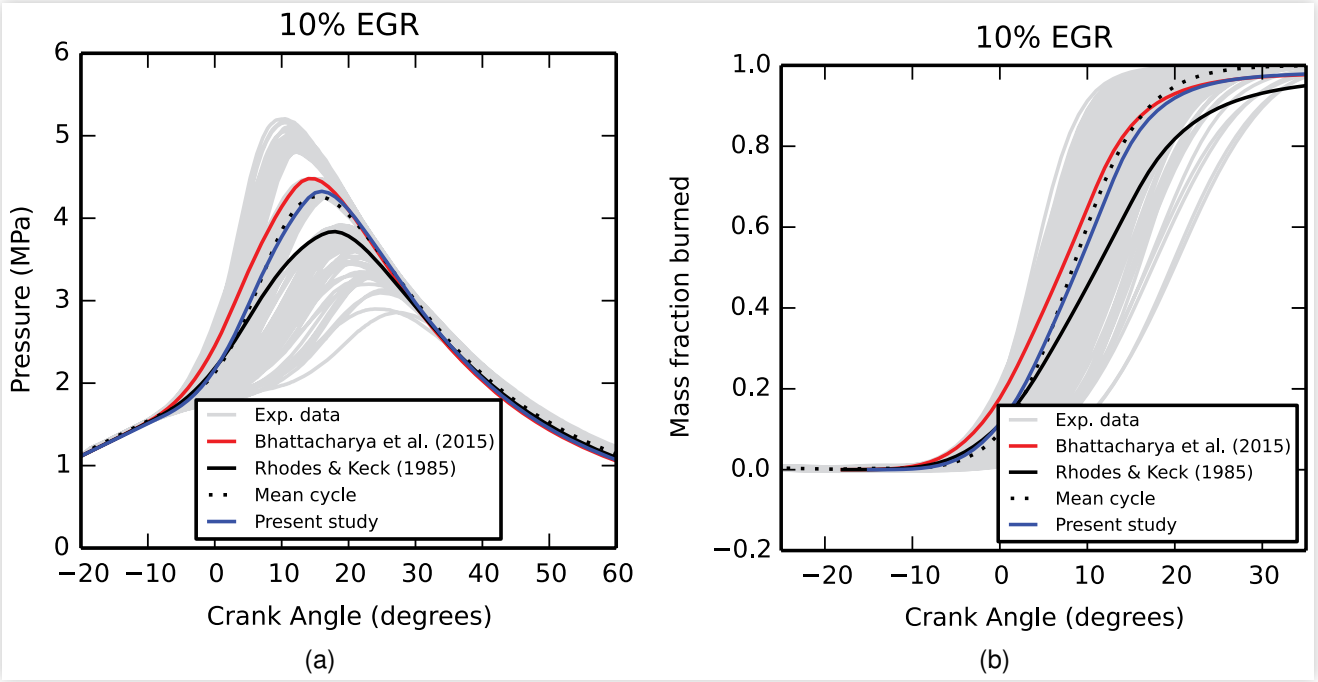

FIGURE 10 Predictive simulations comparing the pressure traces (a) and mass fraction burned (b) at 15% EGR obtained using different EGR correction factor models.

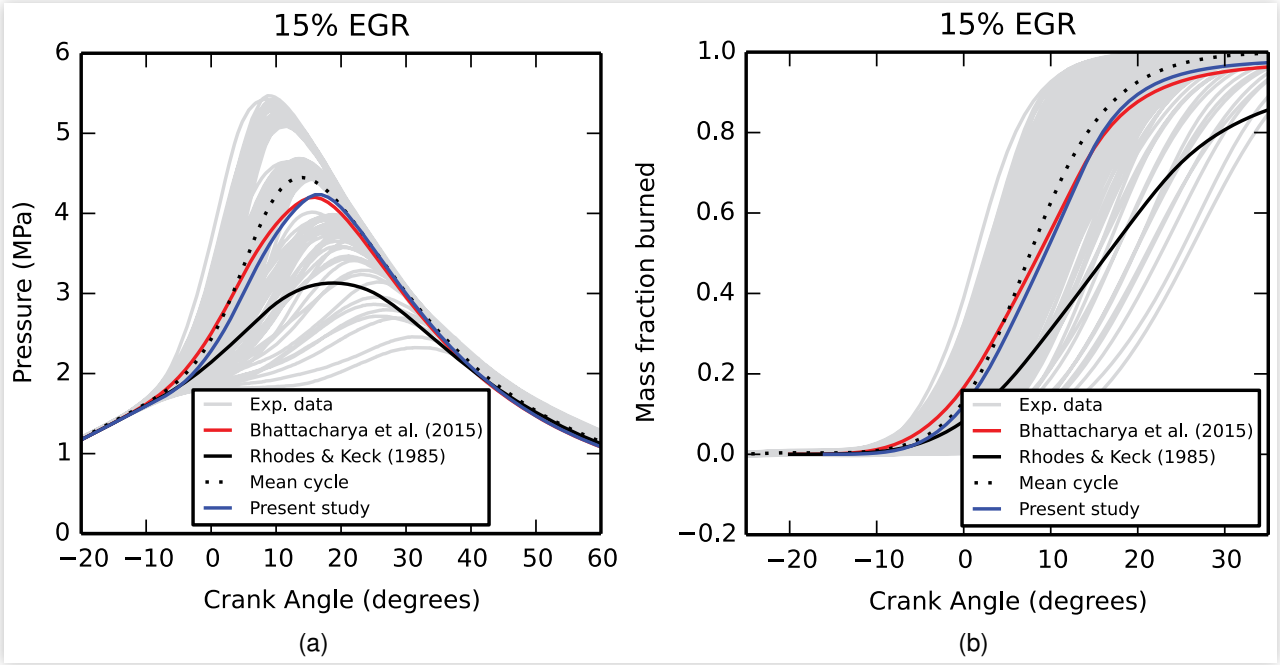

FIGURE 11 Predictive simulations comparing the pressure traces (a) and mass fraction burned (b) at 20% EGR obtained using different EGR correction factor models.

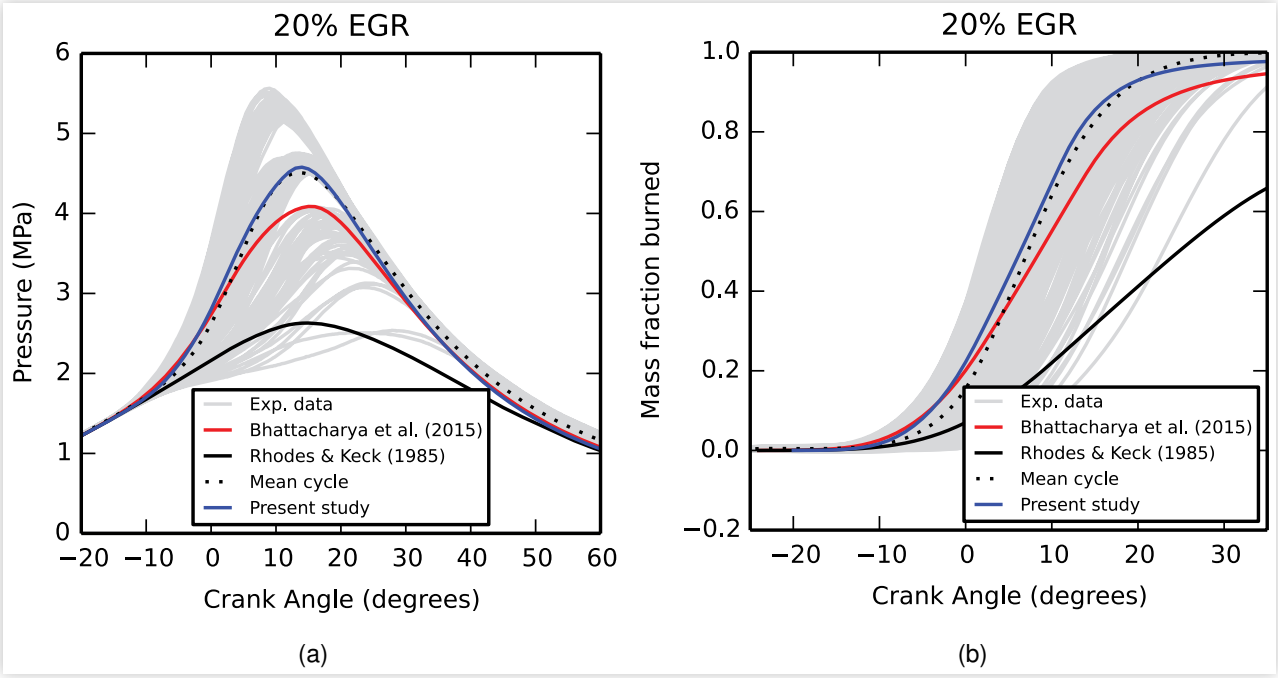

FIGURE 12 Predictive simulations comparing the pressure traces (a) and mass fraction burned (b) at 25% EGR obtained using different EGR correction factor models.

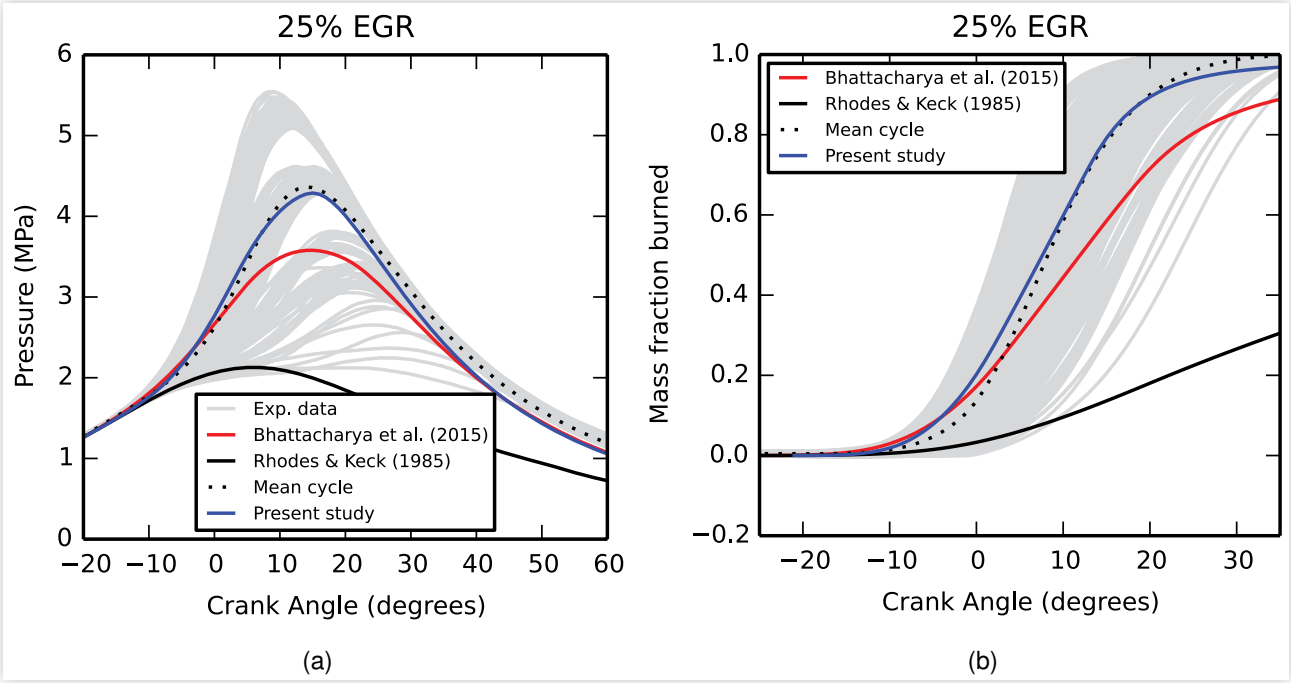

FIGURE 13 RMS error against measured pressure trace for varying levels of EGR for engine speed 1500 rpm and engine load of 0.79 MPa GMEP.

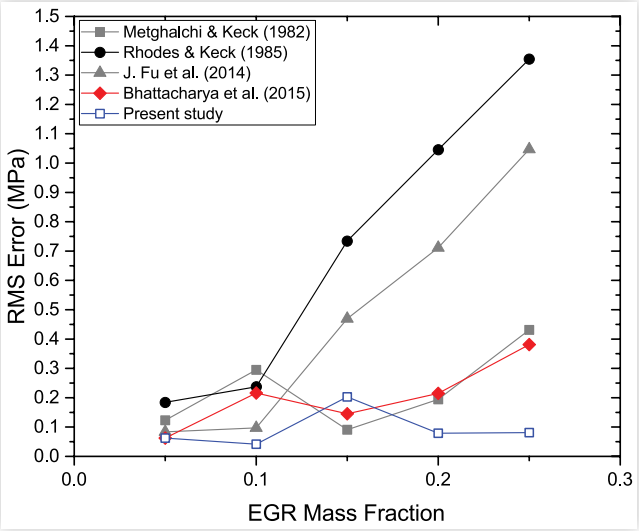

The forward modelling was repeated for part load engine conditions to demonstrate that the new correlation is predictive at engine conditions that are different to those from which it was derived. The zero EGR case was tuned for the part load condition to match a mean cycle. Just as for the full load case, no further tuning was done for the simulations with EGR. The resulting RMS error for the pressure traces are presented in Figure 14. The results show again that the new correlation derived from engine conditions produces the lowest RMS errors across the range of EGR used, matching the results for the full load conditions shown in Figure 13.

FIGURE 14 RMS error against measured pressure trace for varying levels of EGR at 1500 rpm and part load conditions of 0.36 MPa GMEP.

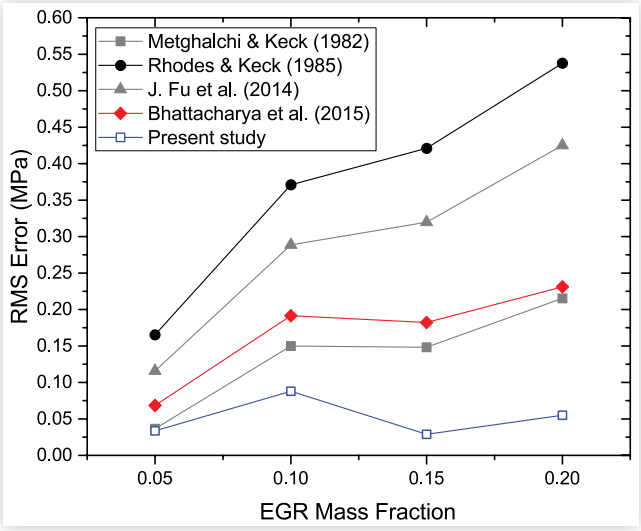

From the four existing models, the Metghalchi and Keck correlation and the Bhattacharya et al. again provide the best predictions across a range of EGR values, whereas Fu et al. and Rhodes and Keck suffer from substantial errors for EGR levels beyond 5%.

Conclusions

The article introduces a new method to determine correction factors for exhaust gas recirculation (EGR) from engine pressure trace data by using a reverse thermodynamic model. Using this approach, a new correlation for the effects of exhaust gas diluent on the laminar burning velocity of a EURO VI specification gasoline is derived and compared against existing models by Metghalchi and Keck [10], Rhodes and Keck [11], Fu et al. [12] and Bhattacharya et al. [14]. It is found that existing models tend to overestimate the impact of EGR on laminar burning velocity, probably because their derivation did not consider all chemical species contained in exhaust gas. This is in agreement with the study by Mannaa et al. [18] who found that synthetic EGR led to a greater reduction in laminar burning velocity when compared to real exhaust gas.

The new correlation and models from the literature were then implemented into a predictive combustion code to compare their predictive modelling capabilities. For the new correlation, simulated pressure traces and mass fraction burned profiles show good agreement with experimental data over the full range of 5%-25% EGR (by mass.) under full load and throttled engine conditions. In contrast, the models by Rhodes and Keck and Fu et al. show reasonable agreement up to 5% EGR but suffer from rapidly rising errors for higher EGR levels. The models by Metghalchi and Keck and Bhattacharaya et al. agree reasonably well even at higher levels of EGR but are outperformed by the new correlation. In line with the too high correction factors, we find that, in the forward model, the four existing correction factors reduce the burning velocity too much, thus tending to model slower combustion cycles instead of mean cycles as EGR increases. For the Rhodes and Keck and Fu et al. model, this effect is particularly pronounced.

Contact Information

Jamie Smith
School of Mechanical Engineering
University of Leeds
Woodhouse Lane, Leeds, LS2 9JT
ed11j5s@leeds.ac.uk

Definitions/Abbreviations

aTDCgx - after top dead centre gas exchange

bTDCgx - before top dead centre gas exchange

CA - Crank Angle
EGR - Exhaust Gas Recirculation
SI - Spark Ignition
RMS - Root Mean Squared
Da - Damköhler number
K - Karlovitz stretch factor
Ma_{sr} - Stretch rate Markstein number
L - Integral length scale
λ - Taylor micro-scale
u_l - Laminar burning velocity
u_t - Turbulent burning velocity

Acknowledgements

Jamie Smith would like to thank Dr Malcolm Lawes for interesting discussions around the *U/K* model and Professor Alexey Burluka for his introduction to the project and valuable supervision during its early stages. Jamie Smith would also like to extend thanks to Jaguar Land Rover for their continued support throughout the project and the University of Leeds for the 110 year anniversary scholarship which made this work possible.

References

1. Takaki, D., Tsuchida, H., Kobara, T., Akagi, M. et al., "Study of an EGR System for Downsizing Turbocharged Gasoline Engine to Improve Fuel Economy," SAE Technical Paper 2014-01-1199, 2014, doi:10.4271/2014-01-1199.
2. Kumano, K. and Yamaoka, S., "Analysis of Knocking Suppression Effect of Cooled EGR in Turbo-Charged Gasoline Engine," SAE Technical Paper 2014-01-1217, 2014, doi:10.4271/2014-01-1217.
3. Alger, T., Gingrich, J., Roberts, C., and Mangold, B., "Cooled Exhaust-Gas Eecirculation for Fuel Economy and Emissions Improvement in Gasoline Engines," *International Journal of Engine Research* 12(3):252-264, 2011, doi:10.1177/1468087411402442.
4. Cairns, A., Fraser, N., and Blaxill, H., "Pre versus Post Compressor Supply of Cooled EGR for Full Load Fuel Economy in Turbocharged Gasoline Engines," SAE Technical Paper 2008-01-0425, 2008, doi:10.4271/2008-01-0425.
5. Cairns, A., Blaxill, H., and Irlam, G., "Exhaust Gas Recirculation for Improved Part and Full Load Fuel Economy in a Turbocharged Gasoline Engine," SAE Technical Paper 2006-01-0047, 2006, doi:10.4271/2006-01-0047.
6. Miller, J., Taylor, J., Freeland, P., Warth, M. et al., "Future Gasoline Engine Technology and the Effect on Thermal Management and Real World Fuel Consumption," SAE Technical Paper 2013-01-0271, 2013, doi:10.4271/2013-01-0271.
7. Grandin, B., Ångstrom, H., Stålhammar, P., and Olofsson, E., "Knock Suppression in a Turbocharged SI Engine by Using Cooled EGR," SAE Technical Paper 982476, 1998, doi:10.4271/982476.
8. Diana, S., Giglio, V., Iorio, B., and Police, G., "A Strategy to Improve the Efficiency of Stoichiometric Spark Ignition Engines," SAE Technical Paper 961953, 1996, doi:10.4271/961953.
9. Edson, M.H., *The Influence of Compression Ratio and Dissociation on Ideal Otto Cycle Engine Thermal Efficiency* (Oxford: Pergamon, 1964), 49-64.
10. Metghalchi, M. and Keck, J., "Burning Velocities of Mixtures of Air with Methanol, Isooctane, and Indolene at High Pressure and Temperature," *Combustion and Flame* 48:191-210, 1982, doi:10.1016/0010-2180(82)90127-4.
11. Rhodes, D. and Keck, J., "Laminar Burning Speed Measurements of Indolene-Air-Diluent Mixtures at High Pressures and Temperatures," SAE Technical Paper 850047, 1985, doi:10.4271/850047.
12. Fu, J., Deng, B., Wang, Y., Yang, J. et al., "Numerical Study and Correlation Development on Laminar Burning Velocities of n-Butanol, Iso-Octane and Their Blends: Focusing on Diluent and Blend Ratio Effects," *Fuel* 124:102-112, 2014, doi:10.1016/j.fuel.2014.01.092.
13. Frassoldati, A., Grana, R., Faravelli, T., Ranzi, E. et al., "Detailed Kinetic Modeling of the Combustion of the Four Butanol Isomers in Premixed Low-Pressure Flames," *Combustion and Flame* 159(7):229311, 2012, doi:10.1016/j.combustflame.2012.03.002.
14. Bhattacharya, A., Banerjee, D.K., Mamaikin, D., Datta, A. et al., "Effects of Exhaust Gas Dilution on the Laminar Burning Velocity of Real-World Gasoline Fuel Flame in Air," *Energy & Fuels* 29(10):6768-6779, 2015, doi:10.1021/acs.energyfuels.5b01299.
15. Luong, M.B., Luo, Z., Lu, T., Chung, S.H. et al., "Direct Numerical Simulations of the Ignition of LeanPrimary Reference Fuel/Air Mixtures with Temperature Inhomogeneities," *Combustion and Flame* 160(10):2038-2047, 2013, doi:10.1016/j.combustflame.2013.04.012.
16. Curran, H.J., Gaffuri, P., Pitz, W.J., and Westbrook, C.K., "A Comprehensive Modeling Study of n-Heptane Oxidation," *Combustion and Flame* 114(1):149-177, 1998, doi:10.1016/S0010-2180(97)00282-4.
17. Curran, H.J., Gaffuri, P., Pitz, W.J., and Westbrook, C.K., "A Comprehensive Modeling Study of Iso-Octane Oxidation," *Combustion and Flame* 129(3):253-280, 2002, doi:10.1016/S0010-2180(01)00373-X.
18. Mannaa, O.A., Mansour, M.S., Roberts, W.L., and Chung, S.H., "Influence of Ethanol and Exhaust Gas Recirculation on Laminar Burning Behaviors of Fuels for Advanced Combustion Engines (FACE-C) Gasoline and Its Surrogate," *Energy & Fuels* 31(12):14104-14115, 2017, doi:10.1021/acs.energyfuels.7b00935.
19. Middleton, R.J., Martz, J.B., Lavoie, G.A., Babajimopoulos, A. et al., "A Computational Study and Correlation of Premixed Isooctane Air Laminar Reaction Fronts Diluted

with EGR," *Combustion and Flame* 159(10):3146-3157, 2012, doi:10.1016/j.combustflame.2012.04.014.

20. Chadwell, C., Alger, T., Zuehl, J., and Gukelberger, R., "A Demonstration of Dedicated EGR on a 2.0 l GDI Engine," *SAE Int. J. Engines* 7(1):434-437, 2014, doi:10.4271/2014-01-1190.
21. Gukelberger, R., Gingrich, J., Alger, T., Almaraz, S. et al., "LPL EGR and D-EGR® Engine Concept Comparison Part 1: Part Load Pperation," *SAE Int. J. Engines* 8(2):570-582, 2015, doi:10.4271/2015-01-0783.
22. Alger, T., Walls, M., Chadwell, C., Joo, S. et al., "The Interaction between Fuel Anti-Knock Index and Reformation Ratio in an Engine Equipped with Dedicated EGR," *SAE Int. J. Engines* (9, 2):786-795, 2016, doi:10.4271/2016-01-0712.
23. Smith, J.K., Roberts, P., Kountouriotis, A., Richardson, D. et al., "Thermodynamic Modelling of a Stratified Charge Spark Ignition Engine," *Int. J. Engine Res.*, online first, 2018, doi:10.1177/1468087418784845.
24. Roberts, P., Kountouriotis, A., Okroj, P., Aleiferis, P. et al., "Effects of Valve Deactivation on Thermal Efficiency in a Direct Injection Spark Ignition Engine under Dilute Conditions," SAE Technical Paper 2018-01-0892, 2018, doi:10.4271/2018-01-0892.
25. Peckham, M., Finch, A., and Campbell, B., "Analysis of Transient HC, CO, NOx and CO2 Emissions from a GDI Engine Using Fast Response Gas Analyzers," *SAE Int. J. Engines* 4(1):1513-1522, 2011, doi:10.4271/2011-01-1227.
26. Cho, H., Lee, K., Lee, J., Yoo, J. et al., "Measurements and Modeling of Residual Gas Fraction in SI Engines," SAE Technical Paper 2001-01-1910, 2001, doi:10.4271/2001-01-1910.
27. Woschni, G., "A Universally Applicable Equation for the Instantaneous Heat Transfer Coefficient in the Internal Combustion Engine," SAE Technical Paper 670931, 1967, doi:10.4271/670931.
28. Heywood, J., *Internal Combustion Engine Fundamentals* Second Edition (New York/London: McGraw-Hill, 1988). ISBN:978-0070286375.
29. Liu, K., Burluka, A.A., and Sheppard, C.G.W., "Turbulent Flame and Mass Burning Rate in a Spark Ignition Engine," *Fuel* 107:202-208, 2013, doi:10.1016/j.fuel.2013.01.042.
30. Aghdam, E.A., "Improvement and Validation of a Thermodynamic SI Engine Simulation Code," Ph.D. thesis, University of Leeds, Leeds, 2003.
31. Conte, E. and Boulouchos, K., "A Quasi-Dimensional Model for Estimating the Influence of Hydrogen-Rich Gas Addition on Turbulent Flame Speed and Flame Front Propagation in IC-SI Engines," SAE Technical Paper 2005-01-0232, 2005, doi:10.4271/2005-01-0232.
32. Verhelst, S. and Sheppard, C.G.W., "Multi-Zone Thermodynamic Modelling of Spark-Ignition Engine Combustion - An Overview," *Energy Conversion and Management* 50(5):1326-1335, 2009, doi:10.1016/j.enconman.2009.01.002.
33. Zimont, V.L., "Theory of Turbulent Combustion of a Homogeneous Fuel Mixture at High Reynolds Numbers," *Combustion, Explosion and Shock Waves* 15:305-311, 1979, doi:10.1007/BF00785062.
34. Lipatnikov, A. and Chomiak, J., "A Simple Model of Unsteady Turbulent Flame Propagation," SAE Technical Paper 972993, 1997, doi:10.4271/972993.
35. Bradley, D., Lawes, M., and Mansour, M.S., "The Problems of the Turbulent Burning Velocity," *Flow, Turbulence and Combustion* 87(2):191-204, 2011, doi:10.1007/s10494-011-9339-y.
36. Bradley, D., Lawes, M., Liu, K., and Mansour, M.S., "Measurements and Correlations of Turbulent Burning Velocities over Wide Ranges of Fuels and Elevated Pressures," *Proceedings of the Combustion Institute* 34(1):1519-1526, 2013, doi:10.1016/j.proci.2012.06.060.
37. Bradley, D., Hicks, R.A., Lawes, M., Sheppard, C.G.W. et al., "The Measurement of Laminar Burning Velocities and Markstein Numbers for Iso-Octane-Air and Iso-Octane-n-Heptane-Air Mixtures at Elevated Temperatures and Pressures in an Explosion Bomb," *Combustion and Flame* 115(1):126-144, 1998, doi:10.1016/S0010-2180(97)00349-0.
38. Bradley, D., Lawes, M., and Mansour, M.S., "Explosion Bomb Measurements of Ethanol-Air Laminar Gaseous Flame Characteristics at Pressures up to 1.4 MPa," *Combustion and Flame* 156(7):1462-1470, 2009, doi:10.1016/j.combustflame.2009.02.007.
39. Blizard, N. and Keck, J., "Experimental and Theoretical Investigation of Turbulent Burning Model for Internal Combustion Engines," SAE Technical Paper 740191, 1974, doi:10.4271/740191.
40. Conway, G.T., " Cyclic Variability of Flame Propagation and Autoignition in Supercharged and Naturally Aspirated SI Engines," Ph.D. thesis, University of Leeds, Leeds, 2013.
41. Khan, A.F., " Chemical Kinetics Modelling of Combustion Processes in SI Engines," Ph.D. thesis, University of Leeds, Leeds, 2014.
42. Aghdam, E.A., Burluka, A.A., Hattrell, T., Liu, K. et al., "Study of Cyclic Variation in an SI Engine Using Quasi-Dimensional Combustion Model," SAE Technical Paper 2007-01-0939, 2007, doi:10.4271/2007-01-0939.

43. Hattrell, T., "A Computational and Experimental Study of Spark Ignition Engine Combustion," Ph.D. thesis, University of Leeds, Leeds, 2007.

44. Robertson, D., Conway, G., Chadwell, C. et al., "Predictive GT-Power Simulation for VNT Matching on a 1.6 L Turbocharged GDI Engine," SAE Technical Paper 2018-01-0161, 2018, doi:10.4271/2018-01-0161.

45. Burluka, A.A., El-Dein Hussin, A.M.T.A., Ling, Z.Y., and Sheppard, C.G.W., "Effects of Large-Scale Turbulence on Cyclic Variability in Spark-Ignition Engine," *Experimental Thermal and Fluid Science* 43:13-22, 2012, doi:10.1016/j.expthermflusci.2012.04.012.